Journal of Power Sources 194 (2009) 1171–1179

Contents lists available at ScienceDirect

Journal of Power Sources

journal homepage: www.elsevier.com/locate/jpowsour

Synthesis, photophysics of two new perylene bisimides and their photovoltaic performances in quasi solid state dye sensitized solar cells

John A. Mikroyannidis[a,*], Minas M. Stylianakis[a], M.S. Roy[c], P. Suresh[b], G.D. Sharma[b,**]

[a] Chemical Technology Laboratory, Department of Chemistry, University of Patras, GR-26500 Patras, Greece
[b] Physics Department, Molecular Electronic and Optoelectronic Device Laboratory, JNV University, Jodhpur 342005 (Raj.), India
[c] Defence Laboratory, Jodhpur 342011 (Raj.), India

ARTICLE INFO

Article history:
Received 3 March 2009
Received in revised form 27 April 2009
Accepted 2 June 2009
Available online 11 June 2009

Keywords:
Perylene bisimide
Anthracene
Pyrene
Photophysics
Quasi solid state dye sensitized solar cell
Electrochemical impedance spectra

ABSTRACT

Two new symmetrical compounds A and P based on perylene-anthracene and perylene-pyrene, respectively, were synthesized and characterized by FT-IR, ^{1}H NMR, TGA and TMA. These compounds contained *tert*-butyl groups which enhanced their solubility, decomposed above 400 °C and gave char yields of 46–65% at 800 °C in N_2. Compound A showed significantly higher glass transition temperature (124 °C) than P (75 °C). Their absorption spectra were broad with longer wavelength absorption at 467–525 nm and optical band gap of 2.05 eV. The solutions of the compounds emitted green-yellow light with maximum at 555 nm, while their films were not photoluminescent. The compound A shows better photovoltaic response than compound P. Quasi solid state dye sensitized solar cells (DSSCs) have been fabricated employing compound A as sensitizer and polymer sol gel as electrolyte and characterized through the current–voltage characteristics in dark as well as under illumination and electrochemical impedance spectra. We found that the Al_2O_3 modification of TiO_2 layer significantly improves the dye absorption resulting in enhancement of power conversion efficiency (PCE) (from 1.15 to 2.13%) which is attributed to the increase in electron lifetime and reduction in back transfer of electrons. Finally, the TiO_2 has been incorporated into the polymer electrolyte gel to improve the power conversion efficiency (3.42%) of the quasi solid state DSSC. The faster electron diffusion in the device, the high ionic conductivity and the low activation energy of the polymer electrolyte are also responsible for enhanced PCE, when TiO_2 nano-particles are incorporated in the polymer electrolyte.

1. Introduction

At present, most successful photovoltaic devices are based on semiconducting materials such as silicon [1], but fabrication cost of these devices is very high. In recent years alternatives to Si based solar cells have been investigated and considerable research is ongoing towards the reduction of the cost of solar cells. Dye sensitized solar cells (DSSCs) have attracted considerable attention in the past few years, since the milestone report by O'Regan and Grätzel [2]. Significant progress has been made to enhance the power conversion efficiency (PCE) employing novel sensitized dyes, electrolytes and photoanode (nano-crystalline metal oxide films) [3–10]. To date, DSSCs based on ruthenium polypyridyl complex sensitized TiO_2 electrodes have shown the highest PCE values in the range of 9–11% [11–13]. However, in view of their cost and environmental problems, metal free dyes are strongly desired. In this context, various organic dyes have been developed for DSSCs [14–18]. In the last few years, increasing research efforts have been devoted to the development of new organic sensitizers and reasonable power conversion efficiencies have been achieved with these dyes [19–21,18,22]. We are interested particularly in perylene bisimide derivatives due to their unique outstanding chemical, thermal and photochemical stabilities [23–25]. So far, several perylene bisimide derivatives sensitized solar cells have been reported, but the PCE values remain low (η = 1.9–2.6) compared with other organic dyes [26–31]. Perylene bisimides are generally poor electron donors, since they are rather used as electron acceptor component in bulk heterojunction photovoltaic devices for photoinduced charge transfer [23,24,32].

Symmetrical perylene bisimides could be synthesized easily in high yield by reactive primary amines in *m*-cresol and isoquinoline. In continuation of our efforts on the development of perylene bisimides for photovoltaic cells, we describe in this article the synthesis of two new symmetrical compounds A and P based on perylene-anthracene and perylene-pyrene, respectively. These compounds were easily synthesized from the condensation

* Corresponding author. Tel.: +30 2610 997115; fax: +30 2610 997118.
** Corresponding author. Tel.: +91 0291 2720857; fax: +91 0291 2720856.
E-mail addresses: mikroyan@chemistry.upatras.gr (J.A. Mikroyannidis), sharmagd_in@yahoo.com (G.D. Sharma).

0378-7753/$ – see front matter © 2009 Elsevier B.V. All rights reserved.
doi:10.1016/j.jpowsour.2009.06.002

of the substituted perylene dianhydride with aminoanthracene and aminopyrene. The compounds carried at the 1,7-bay positions of the perylene central unit, *tert*-butylphenoxy groups which enhanced their solubility. Anthracene [33] and pyrene [34] were inserted as terminal moieties to the molecules of A and P because these species have been used for photovoltaic cells. The thermal and photophysical properties of the compounds were studied. We have explored the possibility of these materials for quasi solid state dye sensitized solar cells. The maximum power conversion efficiency we have achieved is about 1.15% and 2.13% for TiO_2 and Al_2O_3 modified TiO_2 photoelectrodes using polymer electrolyte, which is further enhanced up to 3.42% when TiO_2 nano-filler is added to the polymer electrolyte with Al_2O_3 modified TiO_2 photoelectrode. The enhancement in PCE has been explained in terms of increased electron lifetime, ionic conductivity of polymer electrolyte and low activation energy, when TiO_2 nano-particles are incorporated in the polymer electrolyte.

2. Experimental

2.1. Reagents and solvents

N,*N*-Dimethylformamide (DMF) and tetrahydrofuran (THF) were dried by distillation over CaH_2. All other reagents and solvents were commercially purchased and were used as supplied.

2.2. Characterization methods

FT-IR spectra were recorded on a Perkin-Elmer 16PC FT-IR spectrometer with KBr pellets. ^{1}H NMR (400 MHz) spectra were obtained using a Brucker spectrometer. Chemical shifts (δ values) are given in parts per million with tetramethylsilane as an internal standard. TGA was performed on a DuPont 990 thermal analyzer system. Ground samples of about 10 mg each were examined by TGA and the weight loss comparisons were made between comparable specimens. Dynamic TGA measurements were made at a heating rate of 20 °C min^{-1} in atmospheres of N_2 at a flow rate of 60 cm^3 min^{-1}. Thermo-mechanical analysis (TMA) was recorded on a DuPont 943 TMA using a loaded penetration probe at a scan rate of 20 °C min^{-1} in N_2 with a flow rate of 60 cm^3 min^{-1}. The TMA experiments were conducted at least in duplicate to ensure the accuracy of the results. The TMA specimens were pellets of 10 mm diameter and ~1 mm thickness prepared by pressing powder of sample for 3 min under 8 kPa cm^{-2} at ambient temperature. The T_g is assigned by the first inflection point in the TMA curve and it was obtained from the onset temperature of this transition during the second heating. UV–vis spectra were recorded on a Beckman DU-640 spectrometer with spectrograde THF. The PL spectra were obtained with a Perkin-Elmer LS45 luminescence spectrometer. The PL spectra were recorded with the corresponding excitation maximum as the excitation wavelength. Elemental analyses were carried out with a Carlo Erba model EA1108 analyzer.

2.3. Preparation of compounds

2.3.1. 1,7-Dibromo-3,4,9,10-perylenetetracarboxylic dianhydride (**1**)

Compound **1** was prepared by bromination of 3,4,9,10-perylenetetracarboxylic dianhydride using bromine and a catalytic amount of iodine in sulfuric acid [35]. The 1,7-dibromoderivative is the predominant isomer which was obtained as reaction product.

2.3.2. 1,7-(4-tert-Butylphenoxy)perylene-3,4,9,10-tetracarboxylic dianhydride (**2**)

Compound **2** was prepared from the condensation of **1** with 4-*tert*-butylphenol in DMF in the presence of K_2CO_3 [36].

2.3.3. 9-Nitroanthracene (**3**)

Compound **3** was prepared from the nitration of anthracene by means of concentrated nitric acid in glacial acetic acid [37]. It was purified by recrystallization from methanol.

2.3.4. 9-Aminoanthracene (**4**)

Compound **4** was prepared from the reduction of **3** using hydrazine monohydrate in ethanol in the presence of a catalytic amount of Pd/C [37].

2.3.5. 2- and 4-nitropyrene (**5**)

Compound **5** was prepared according to a reported method [38] which was modified as follows. A flask was charged with a mixture of pyrene (1.00 g, 4.94 mmol) and glacial acetic acid (30 ml). The mixture was heated at about 60 °C to dissolve the pyrene. To this warm solution concentrated nitric acid 63% (0.49 g, 4.94 mmol) dissolved in glacial acetic acid (~5 ml) was added dropwise with vigorous stirring. An exothermic reaction was observed and the product precipitated as yellowish solid. Stirring of the mixture at room temperature was continued for 4 h. It was subsequently poured into ice-water. The solid was filtered off, washed thoroughly with water and dried. It was purified by recrystallization from ethanol (0.73 g, 63%). A mixture of 2- and 4-nitropyrene was obtained from this reaction according to the literature [38].

2.3.6. 2- and 4-aminopyrene (**6**)

Compound **6** was prepared according to a reported method [39] which was modified as follows. A flask was charged with a solution/suspension of **5** (0.29 g, 1.17 mmol) in ethanol (20 ml). A catalytic amount (~0.2 g) of 10% Pd/C was added to the mixture. It was subsequently heated to reflux, and 3 ml of hydrazine monohydrate was added slowly at reflux temperature. After a further 12 h of reflux, the solution was filtered to remove the catalyst, the filtrate was concentrated in a rotary evaporator and the concentrate was cooled into a refrigerator. The pale green precipitate was filtered, washed with water and dried to afford a mixture of 2- and 4-aminopyrene. The crude product was recrystallized from ethanol (0.18 g, 72%).

2.3.7. Compound A

A flask was charged with a mixture of **2** (0.1000 g, 0.145 mmol) and DMF (25 ml). The mixture was heated to dissolve compound **2**. To this solution, compound **4** (0.0561 g, 0.290 mmol) and glacial acetic acid (0.041 g, 0.683 mmol) were added. The mixture was stirred and heated at 130 °C for 18 h under N_2. It was subsequently concentrated under reduced pressure and the concentrate was poured into water. The brown-black precipitate was filtered, washed with water and dried to afford A (0.1293 g, 78%).

FT-IR (KBr, cm^{-1}): 3038, 2956, 1656, 1622, 1592, 1508, 1400, 1266, 1236.

^{1}H NMR (DMSO-d_6) ppm: 8.56–8.10 (m, 16H, perylene protons and anthracene protons at positions 1,4,5,8,10); 7.94–7.83 (m, 8H, anthracene protons at positions 2,3,6,7); 7.32 (m, 4H, phenylene protons *meta* to oxygen); 7.03 (m, 4H, phenylene protons *ortho* to oxygen); 1.20 (s, 18H, aliphatic protons of *tert*-butyl).

Anal. Calcd. for $C_{72}H_{50}N_2O_6$: C, 83.22; H, 4.85; N, 2.70. Found: C, 82.10; H, 4.12; N, 3.06.

2.3.8. Compound P

Compound P was similarly prepared as a brown-black solid in 70% yield from the reaction of **2** with **6** in DMF in the presence of glacial acetic acid.

FT-IR (KBr, cm^{-1}): 3040, 2958, 1654, 1638, 1592, 1508, 1396, 1268, 1236, 840, 714.

^{1}H NMR (DMSO-d_6) ppm: 8.56–7.82 (m, 24H, perylene and pyrene protons); 7.32 (m, 4H, phenylene protons *meta* to oxygen);

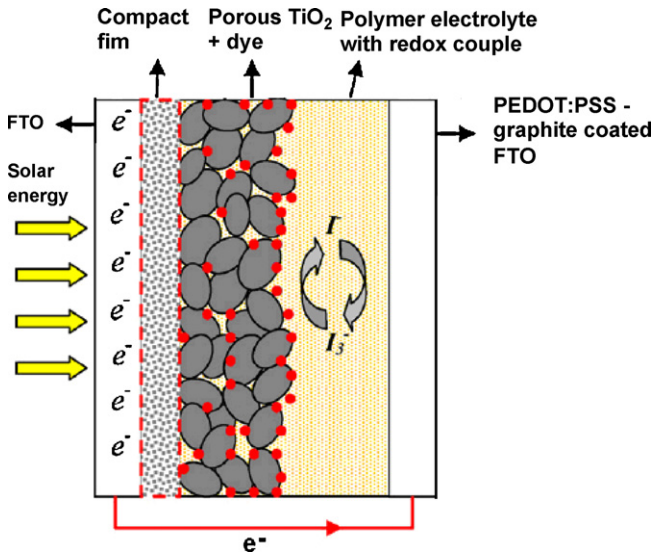

Fig. 1. Schematic diagram of quasi solid state DSSC with compact TiO_2 layer, porous TiO_2 + dye, polymer electrode with redox couple and PEDOT:PSS-graphite coated FTO counter electrode.

7.03 (m, 4H, phenylene protons *ortho* to oxygen); 1.20 (s, 18H, aliphatic protons of *tert*-butyl).

Anal. Calcd. for $C_{76}H_{50}N_2O_6$: C, 83.96; H, 4.64; N, 2.58. Found: C, 82.57; H, 5.16; N, 3.10.

2.4. Dye sensitized solar cell preparation and characterization

The following devices were fabricated: (A) FTO/compact TiO_2 layer/np-TiO_2–perylene dye/polymer electrolyte/counter electrode, (B) FTO/compact TiO_2 layer/Al_2O_3 modified np-TiO_2–perylene dye/polymer electrolyte/counter electrode, and (C) FTO/compact TiO_2 layer/Al_2O_3 modified np-TiO_2–perylene dye/TiO_2 nano-filler:polymer electrolyte/counter electrode. The configuration of device C is same as device B except the polymer electrolyte with TiO_2 has been used.

A TiO_2 colloidal dispersion was prepared by adding 10 ml of deionized water to 3 g of P_{25} powder (Degussa product). Further, 0.25 ml of acetylacetone was added to prevent the re-aggregation of TiO_2 particles, followed by a 20 min sonication; 0.13 ml of detergent (Triton X-100) was introduced to facilitate spreading of the dispersion on to the substrates. FTO conducting glass substrates were cleaned with deionized water rinsed with 2-iso-propanol and dried in ambient condition. A thin compact layer of TiO_2 film (approximately 10 nm thickness) was deposited on the FTO glass substrates by means of dip coating in order to improve the ohmic contact and adhesion between porous TiO_2 and FTO substrates [40]. The above colloidal dispersion was spread on the surface of compact film by means of the doctor blading technique. The thickness of the porous layer was controlled by an adhesive tape. Thereafter, the film was sintered at 450 °C for 30 min in air. The thickness of the obtained porous film was approximately 6 μm. After cooling the electrodes to room temperature, the electrodes were immersed in 5×10^{-4} M dye solution in THF overnight at room temperature.

The counter electrode was made by developing a thin film of protonated poly-(3,4-ethylenedioxythiophene)-polystyrene (PEDOT:PSS) over graphite coated FTO glass substrates. In this process, first the FTO is coated with graphite and then DMSO treated PEDOT:PSS was grown over the top of the film by dip coating method. The film was treated dried at 80 °C for 30 min.

After sensitization, a quasi solid state polymer electrolyte 0.5 M KI/0.05 I_2, 0.26 g of PEO and 44 μl of 4-*tert*-butylpyridine in 1:1 acetone/propylene carbonate was spread on the dye sensitized TiO_2 film by spin coating to form a hole conducting layer. To incorporate the nano-fillers in the polymer electrolyte 0.038 g of TiO_2 (P_{25}

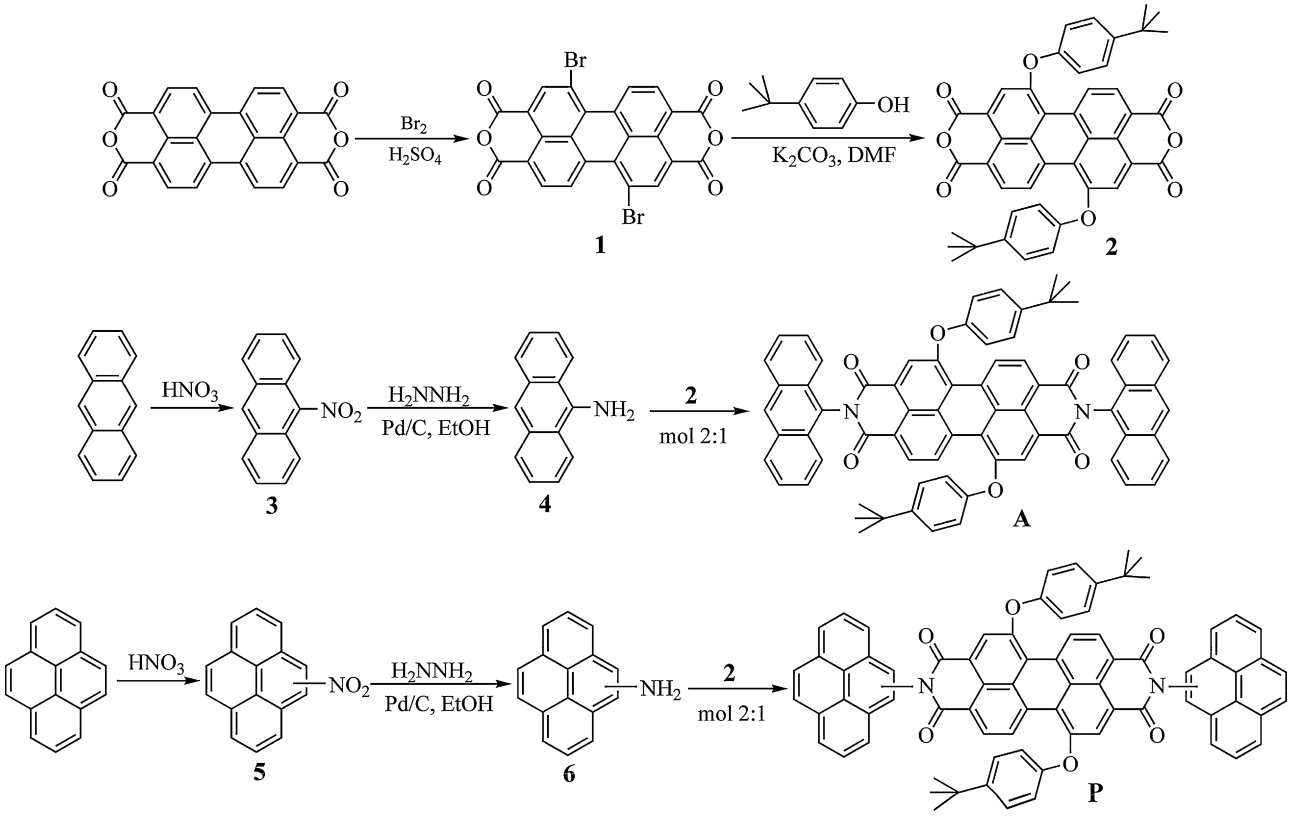

Scheme 1. Synthesis of compounds A and P.

Degussa) powder was added to it. The cells were made by clamping the photoanode consisting of polymer electrolyte with counter electrode. The systematic structure of the quasi solid state dye sensitized solar cell is shown in Fig. 1.

The TiO_2 surface modification by Al_2O_3 was performed as follows: a nano-porous TiO_2 electrode was dipped into a solution of $Al(OC_3H_7)_3$ for 10 min and then rinsed with deionized water and dried in air for 1 h. This procedure was repeated for two times followed by the sintering at 450 °C for 30 min in air.

The electrochemical impedance spectra (EIS) measurements were carried out by applying bias of the open circuit voltage (V_{oc}) and recorded over a frequency range of 1 mHz to 10^5 Hz with ac amplitude of 10 mV. The above measurements were recorded with an Autolab Potentiostat PGSTAT-10 equipped with frequency response analyzer (FRA). The current–voltage (J–V) characteristics in dark and under illumination were obtained by a Keithley electrometer.

3. Results and discussion

3.1. Synthesis and characterization

Scheme 1 outlines the synthesis of compounds **1** [35], **2** [36], **3** [37], **4** [37], **5** [38] and **6** [39] according to the literature. The nitration of pyrene by means of an equivalent amount of nitric acid in glacial acetic acid affords a mixture of 2- and 4-nitropyrene [38] which were not isolated since their properties are expected to be similar. Therefore, compounds **5**, **6** and P were obtained as a mixture of two isomers. Compounds A and P were soluble in polar organic solvents such as THF, chloroform, and dichloromethane due to the presence of the *tert*-butyl groups. Even though these compounds are monomers, thin films of them could be obtained from THF solutions by spin-casting.

The FT-IR spectra of compounds showed certain characteristic absorption bands which for A appeared at 3038 (aromatic C–H stretching); 2956 (C–H stretching of *tert*-butyl groups); 1656, 1622 (carbonyl stretching); 1592, 1508 (aromatic breathing modes); 1400 (C–H deformation of *tert*-butyl groups) and 1266, 1236 cm^{-1} (ether bond). Fig. 2 depicts the ^1H NMR spectra of A and P. Compound A displayed an upfield signal at 8.56–8.10 ppm assigned to the perylene protons labelled "d". The aromatic protons "e", "b" and "c" resonated at 7.94–7.83, 7.32 and 7.03 ppm, respectively, while the *tert*-butyl protons gave a singlet at 1.20 ppm. Compound P showed multiplets at the region of 8.56–7.82 ppm assigned to the perylene and pyrene protons. Finally, the protons "b", "c" and "a" gave similar resonances with those of the corresponding protons of A.

Thermal characterization of compounds was accomplished by TGA and TMA (Fig. 3). The decomposition temperature (T_d) and the char yield (Y_c) at 800 °C by TGA as well as the glass transition temperature (T_g) by TMA are listed in Table 1. Both compounds were stable up to ~300 °C, had T_d values of 400–427 °C and Y_c of 46–65%. The T_g was 124 °C for A and 75 °C for P. The anthracene ring seems to render the molecule of A more rigid relative to pyrene of P.

3.2. Photophysical properties

Fig. 4 presents the normalized UV–vis absorption spectra A and P in dilute (10^{-5} M) THF solution and thin film. Fig. 5 depicts their emission photoluminescence (PL) spectra in THF solution. The PL spectra in thin films were not recorded because they were not photoluminescent to a detectable extend. Table 1 summarizes all photophysical characteristics.

The absorption spectra (Fig. 4) were broad and covered a significant part of the visible region from 300 nm up to about 550 nm

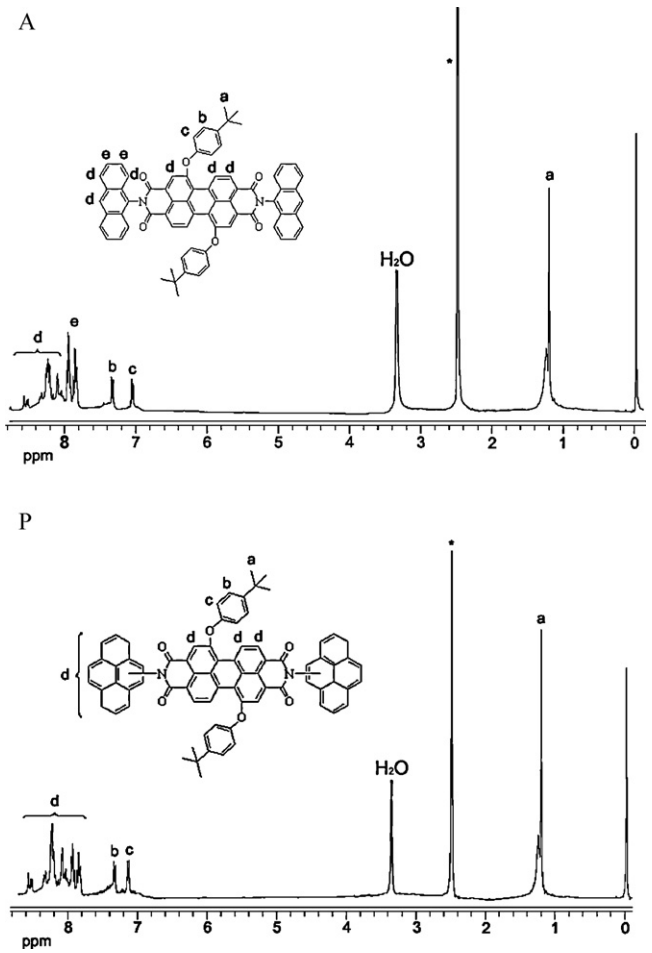

Fig. 2. ^1H NMR spectra in DMSO-d_6 solution of compounds A (top) and P (bottom). The solvent peak is denoted by an asterisk.

in solutions and 600 nm in thin films. The shorter wavelength absorption maximum ($\lambda_{a,max}$) was located around 340 nm and corresponds to n–π* transitions. The longer wavelength $\lambda_{a,max}$ was at 467–525 nm and is assigned to the π–π* transitions. The absorption curves of A and P were similar in both solution and thin film thus indicating that the chemical structure of the terminal units (anthracene and pyrene) did not influence considerably

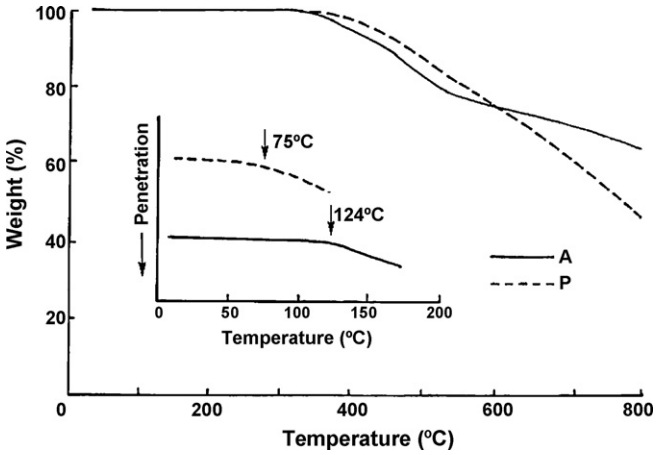

Fig. 3. TGA thermograms of compounds A and P in N_2. The insert shows the TMA traces of these compounds. Conditions: N_2 flow, 60 cm^3 min^{-1}; heating rate, 20 °C min^{-1}.

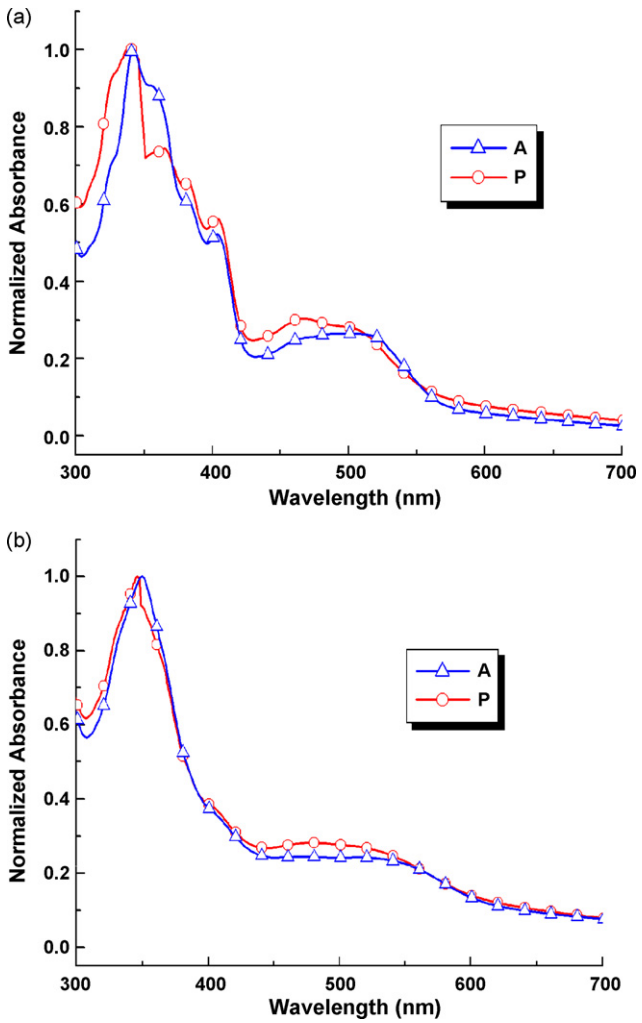

Fig. 4. Normalized UV–vis absorption spectra of compounds A and P in 10^{-5} M THF solution (a) and thin film (b).

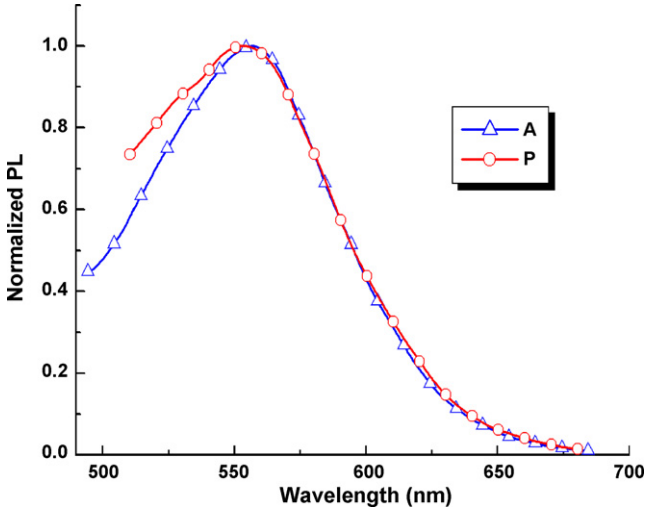

Fig. 5. Normalized PL emission spectra of compounds A and P in THF solution by photoexcitation at 470 nm.

Table 1
Thermal and optical properties of compounds A and P.

	Compound	
	A	P
T_d [a] (°C)	400	427
Y_c [b] (%)	65	46
T_g [c] (°C)	124	75
$\lambda_{a,max}$ [d] in THF solution (nm)	510	467
$\lambda_{f,max}$ [e] in THF solution (nm)	555	555
$\lambda_{a,max}$ [d] in thin film (nm)	525	476
E_g^{opt} [f] (eV)	2.05 (606 nm)[g]	2.05 (606 nm)[g]

The PL emission spectra were recorded at 470 nm excitation wavelength.
[a] Decomposition temperature corresponding to 5% weight loss in N_2 determined by TGA.
[b] Char yield at 800 °C in N_2 determined by TGA.
[c] Glass transition temperature determined by TMA.
[d] The absorption maxima from the UV–vis spectra in THF solution or in thin film.
[e] The PL maxima in THF solution.
[f] The optical band gap calculated from the onset of the thin film absorption.
[g] Numbers in parentheses indicate the onset of the thin film absorption.

their absorption. The thin film absorption onset was identical for both compounds and was located at 606 nm which corresponds to an optical band gap (E_g^{opt}) of 2.05 eV. Thus from the respect of absorption, both compounds seems to be almost equivalent. An E_g^{opt} value of about 2.0 eV has been reported for donor–acceptor type thiophene–perylene–thiophene polymers [36]. Furthermore, oligothiophene-functionalized perylene bisimide systems have displayed E_g^{opt} of 1.97–1.63 eV [41].

The solutions of A and P emitted green-yellow light, when they were photoexcited at the excitation maximum (470 nm). Again the PL emission curves (Fig. 5) were similar with maximum ($\lambda_{f,max}$) at 555 nm for both compounds.

3.3. Characterization of TiO_2 films

The X-ray patterns of the compact (C) porous film (P) and compact–porous (CP) film are shown in Fig. 6. Anatase and rutile phase peaks are marked as A and R, respectively in this figure. It is observed that the C film consists only of pure anatase phase showing only diffraction peaks corresponding to the anatase phase. However, P film and CP film show both anatase and rutile phases. The XRD patterns and relative intensity of P and CP films were almost the same.

Fig. 7 shows the UV–vis absorption spectra for the perylene dye absorbed TiO_2 films with and without Al_2O_3 modification. It reveals that the modification of Al_2O_3 apparently increases the amount of adsorbed dye molecules. To further confirm the surface concentration of perylene dye, the dye was desorbed from the TiO_2 surface into 0.05 NaOH solution and the absorption spectrum was measured. The result showed that the surface concentration of dye increases from 6.85×10^{-8} to 9.6×10^{-8} mol cm^{-3} upon the Al_2O_3

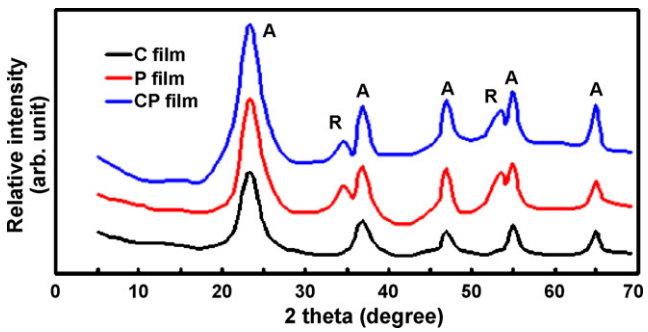

Fig. 6. XRD spectra of C, P and CP films.

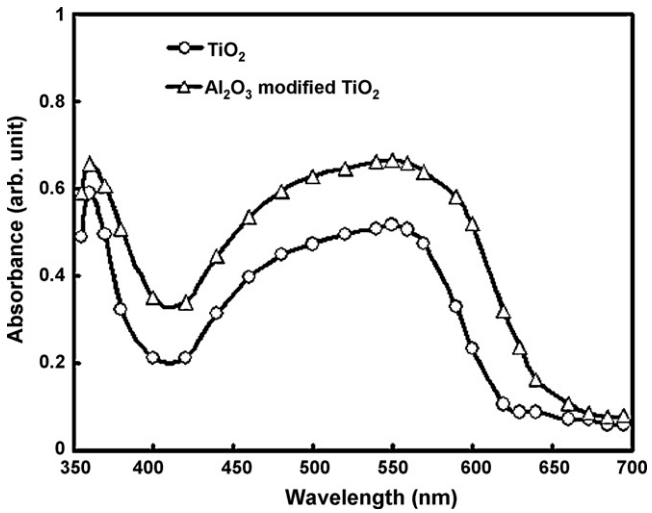

Fig. 7. UV–vis absorption spectra of perylene compound A adsorbed TiO_2 photoelectrodes.

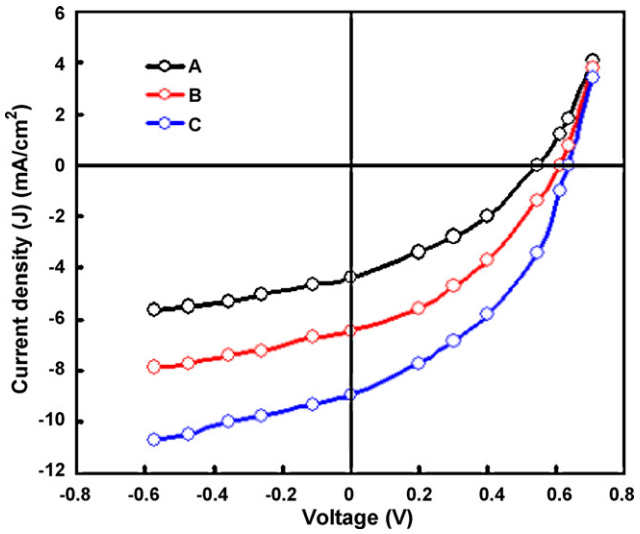

Fig. 8. Current–voltage characteristics of DSSCs under illumination of 100 mW cm^{-2}.

modification. The higher concentration is attributed to the higher basicity of the TiO_2 film upon Al_2O_3 modification. If the modification material is more basic than TiO_2, the imide carbonyl groups in the perylene dye molecules are more easily adsorbed to the surface of the coating layer [42]. It is also observed that the maximum absorption peak at 550 nm for perylene dye, which is assigned to π–π^* transition, blue shifts by 12 nm to 538 nm upon Al_2O_3 modification. The blue shift of the π–π^* transition peak results from the increased surface basicity due to Al_2O_3 modification.

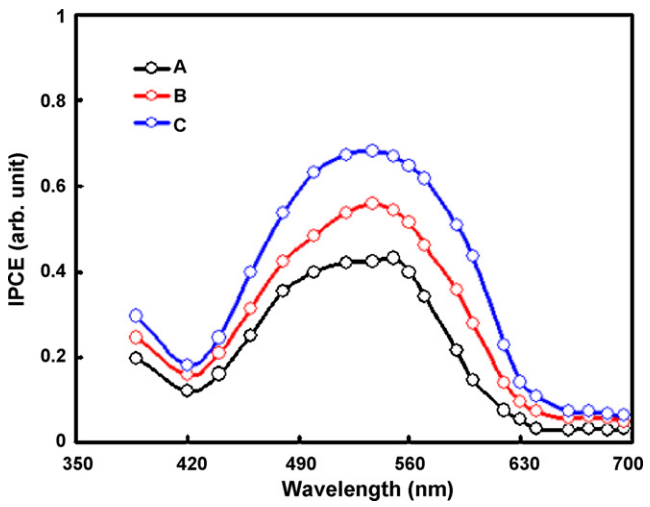

Fig. 9. IPCE spectra of DSSCs.

3.4. Photovoltaic properties

Fig. 8 shows the current–voltage characteristics for A, B and C devices under illumination of intensity 100 mW cm^{-2}. Table 2 shows the comparison of the photovoltaic performance of the devices. The IPCE spectra of the devices are shown in Fig. 9. As it can be seen, the IPCE is higher for the DSSCs fabricated from the photoelectrode with Al_2O_3 modified TiO_2 photoelectrode than that for unmodified TiO_2 electrode. The IPCE can be expressed in terms of the light harvesting efficiency (LHE), the quantum yield of the charge injection (ϕ_{inj}), and the efficiency (η_c) of collecting the injected charge at back contact as shown in the following expression:

$$\text{IPCE} = \text{LHE}(\lambda)\phi_{inj}\eta_c$$

The LHE is mainly proportional to the adsorbed dye molecules per square centimeter, ϕ_{inj} and η_c are related to the crystallinity of the TiO_2 nano-particles. Additionally, η_c is directly determined by the film resistance and electron lifetime (τ_n). As it can be seen from the optical absorption spectra of the dye sensitized photoelectrodes, the absorption intensity is higher for the Al_2O_3 modified TiO_2 electrode than that for unmodified TiO_2 photoelectrode (Fig. 7). Therefore, for the electrode with modified TiO_2, the LHE (λ) may be greater, due to the higher adsorbed amount of perylene dye molecules. But, the overall improvement in the IPCE is not only due to this phenomenon. Al_2O_3 has been used as modification material of TiO_2 photoanode, since layer of Al_2O_3 can form insulat-

Table 2
Comparison of photovoltaic performance for DSSCs A, B and C.

Device	Short circuit current, J_{sc} (mA cm^{-2})	Open circuit voltage, V_{oc} (V)	Fill factor, FF	Power conversion efficiency, η (%)
Device A: FTO/compact TiO_2 layer/np-TiO_2–perylene dye/polymer electrolyte/counter electrode	4.37	0.54	0.49	1.15
Device B: FTO/compact TiO_2 layer/Al_2O_3 modified np-TiO_2–perylene dye/polymer electrolyte/counter electrode	6.45	0.61	0.54	2.13
Device C: FTO/compact TiO_2 layer/Al_2O_3 modified np-TiO_2–perylene dye/TiO_2 nano-filler:polymer electrolyte/counter electrode	8.92	0.65	0.59	3.42

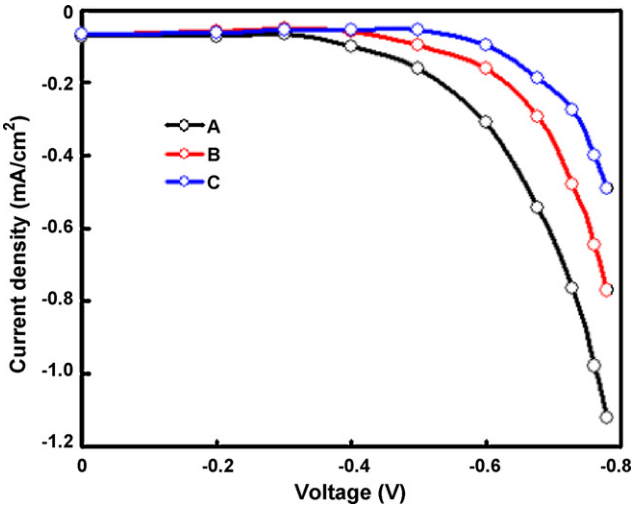

Fig. 10. Dark current–voltages curves for DSSCs A, B and C.

ing barrier at the TiO_2/dye interface because of its higher band gap compared with TiO_2 and also at the same time a physical separation of injected electrons from the oxidized dye/redox couple in the electrolyte [43,44]. Therefore, the increase in IPCE and power conversion efficiency for the device B was attributed to the reduction in recombination reaction occurring in the DSSCs.

The dark current–voltage curves in Fig. 10 showed that the dark current onset shifted to a larger potential for DSSCs with modified TiO_2 electrode. The dark current value at the same potential decreased for device B. This observation indicated that the Al_2O_3 retarded the charge recombination. Therefore, the photovoltage was enhanced and the dark current was reduced. The modification of Al_2O_3 not only generates a barrier that reduces the dark current but also shifts the conduction band potential in negative direction, revealing a lower electron density at any applied potential [45]. Consequently, at each applied potential, the back transfer of electrons in modified TiO_2 is lower than that in unmodified TiO_2. From the dark current measurements, it can be concluded that the resistance of TiO_2 increases as a result of the negative shift of TiO_2 conduction band potential [46].

3.5. Electrochemical impedance spectral properties

The present QSDSC were investigated by electrochemical impedance spectroscopy (EIS) performed at open circuit voltage of each solar cell under illumination. EIS has proven to be a useful technique for the characteristics of electronic and ionic processes in DSSCs [47–49]. The impedance analysis of solar cells composed of unmodified Al_2O_3 and modified TiO_2 photoelectrodes was performed at V_{oc} of each cell under illumination. Fig. 11(a) shows Nyquist plots of the DSSCs. Three arcs are observed in the frequency regime of 10^3–10^5, 1–10^3 and 0.1–1 Hz, from left to right. These arcs are associated with (i) the charge transfer process at the interface between counter electrode and redox couple (high frequency), (ii) the transport process of injected electrons within the photoelectrode film and the charge transfer process of the injected electrons at the interface between the photoelectrode and electrolyte/dye coating (middle frequency), and (iii) the diffusion of I_3^-/I^- redox couple within the electrolyte (low frequency). Identical semicircle for high frequency region indicates that the modification of photoelectrode does not impact the charge transfer at counter electrode/electrolyte interface. As expected there is no change in the low frequency arc, because the photoanode is modified before the fabrication of device. It is observed that the semicircle of the middle frequency region of the cell based on modified TiO_2 photoelectrode

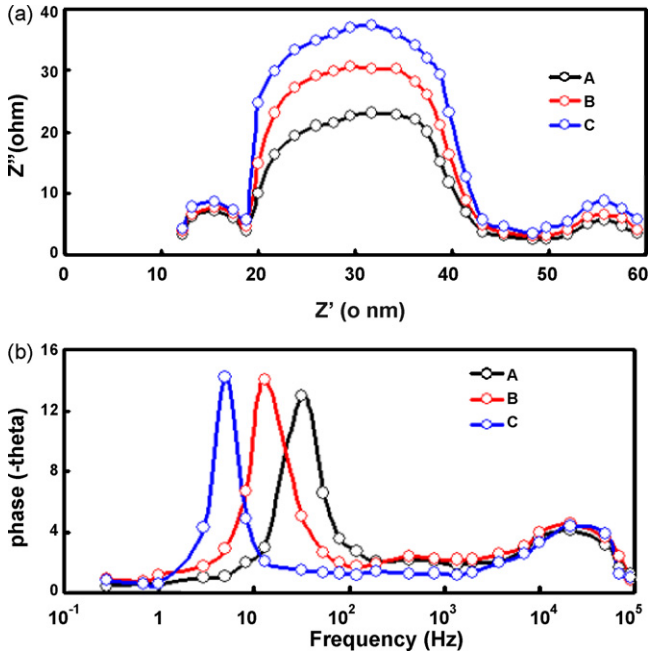

Fig. 11. (a) Nyquist plot and (b) Bode plots of EIS spectra for DSSCs A, B and C.

gets larger than the unmodified TiO_2 photoelectrode. At open circuit, the electrons, which are injected from the adsorbed dye to the photoelectrode partially accumulate at the interface at photoelectrode/dye/electrolyte and react with the electrolyte, thereby decreasing the impedance of this region. Therefore, the larger semicircle for modified TiO_2 photoelectrode shows that the recombination of the photogenerated electron with electrolyte by the backward transfer is retarded by the photoelectrode. The electrons injected from the dye into the conduction band of photoelectrode are efficiently extracted by the photoelectrode with modified TiO_2 as compared to TiO_2 photoelectrode. This was also confirmed from dark current measurements, in which the dark current is reduced for the DSSC with modified TiO_2 photoelectrode.

The Bode plots of DSSCs with modified and unmodified TiO_2 photoelectrodes are illustrated in Fig. 11(b). Two peaks associated with the transfer of photogenerated electrons at the surface of photoelectrodes and conducting electrodes, are clearly observed. According to the EIS model developed by Kern et al. [50], the lifetime of injected electron from the dye to photoelectrode film can be drawn from the position of the low frequency peak in Fig. 11(b) through the expression $\tau = 1/2\pi f$, where f is the frequency of the superimposed ac voltage. The peak frequency in the Bode plot for DSSC with modified photoelectrode is about 20% smaller than that for TiO_2 photoelectrode. This indicates that the electron lifetime (14 ms) increases (14 ms from 8 ms for unmodified TiO_2 photoelectrode) when the modified photoelectrode is used in DSSC having the same dye and electrolyte. This also confirms the retard reaction of electrons with I_3^- in the electrolyte.

3.6. Effect of np-TiO_2 nano-fillers in the polymer electrolyte

We have investigated the effect of the incorporation of TiO_2 nano-particles in the solid electrolyte on charge transport and on the photovoltaic response a quasi solid state DSSC using modified TiO_2 photoelectrode. The current–voltage characteristics of the devices are shown in Fig. 8. It is observed that the short circuit current (J_{sc}) (8.9 mA cm^{-2}) is significantly enhanced by the incorporation of TiO_2 nano-particles in the polymer electrolyte, without a significant change in open circuit voltage (V_{oc}). The J–V

characteristics in dark (Fig. 10) show that nano-fillers in the polymer electrolyte cause a reduction in the dark current. This may be due to the lower concentration of free tri-iodide ions near the dye-sensitized TiO_2 surface because the surfaces of the nano-filler can immobilize these ions. This also results in slightly smaller V_{oc} due to the high electron concentration at the TiO_2 surface of electrolyte. The charge transport in electrolyte medium may be effectively facilitated by adding nano-particles to the polymer electrolyte. The enhanced ion mobility of the nano-particles polymer electrolyte gel may be explained by an ion exchange mechanism with the formation of an electron transport path [51,52]. We have also measured the EIS spectra of the quasi solid state DSSC under illumination at a bias voltage equal to open circuit voltage of the cells. Similar results were observed as shown in Fig. 11. It was observed that the impedance in low frequency range is significantly reduced by the nano-particles in the polymer electrolyte due to the improved ion mobility. The electron lifetime calculated from the Bode plots of impedance spectra is about 21 ms for this device. The DSSC based on TiO_2–polymer electrolyte shows the longer electron lifetime mostly due to the reduction in dark current.

The IPCE curves of quasi solid state DSSCs are shown in Fig. 9. The introduction of nano-filler induces a significant improvement in IPCE throughout the whole wavelength region. The overall power conversion efficiency of the quasi solid state DSSC with the electrolyte containing TiO_2 nano-particles is about 3.2%. This suggest that the enhancement in the solar cell performance upon the introduction of the TiO_2 nano-fillers in the polymer electrolyte is due to the improved ion conductivity, light scattering and enhancement in the electron lifetime.

We have investigated the ionic conductivity of the polymer electrolyte with and without TiO_2 nano-particles in it as a function of temperature ranging from room temperature to 100 °C. The ionic conductivity (σ) of the polymer electrolyte was estimated from the EIS data using the following expression [53,54]:

$$\sigma = \frac{L}{R_b A}$$

where R_b is the bulk resistance, L and A are the device dimensions i.e. thickness and area, respectively. The value of R_b is calculated from the intersection of prolongation of the high frequency line, to the real impedance axis, in EIS measurement. At room temperature, the ionic conductivity of the polymer with and without TiO_2 nano-particles is 1.5 and 2.1 mS cm^{-1}, respectively and increases with the temperature because the transportation of the ions becomes faster at higher temperatures. Fig. 12 shows the variation of the ionic conductivity of the polymer electrolyte with temperature. The data in the Fig. 10 can be well fitted by Arrhenius equation:

$$\sigma(T) = A \exp\left(\frac{-E_a}{kT}\right)$$

where A is a constant, E_a the activation energy, K is Boltzmann constant, and T is the absolute temperature. The activation energy of the polymer electrolyte with and without TiO_2 is 0.18 and 0.14 eV, respectively. The higher ionic conductivity and lower activation energy of polymer electrolyte with TiO_2 indicates the improved ionic conduction, thereby resulting the PCE of the DSSC with polymer electrolyte with TiO_2 nano-particles.

The electron diffusion coefficient (D_n) has been estimated from the EIS spectra as shown in Fig. 11(a) using $D_n = L^2/R_t C_\mu$, where L is the thickness of the DSSC, R_t is the electron transport resistance, and C_μ is chemical potential. The values of R_t and C_μ have been estimated from the arc in the middle frequency region of the Nyquist plots [55,56]. The estimated values of D_n for device B and C are 5.2×10^{-5} and 6.7×10^{-5} cm^2 s^{-1}, respectively. The higher value of D_n for device C indicates the faster diffusion of electrons in this device, which is in fact responsible for the improved PCE for device C.

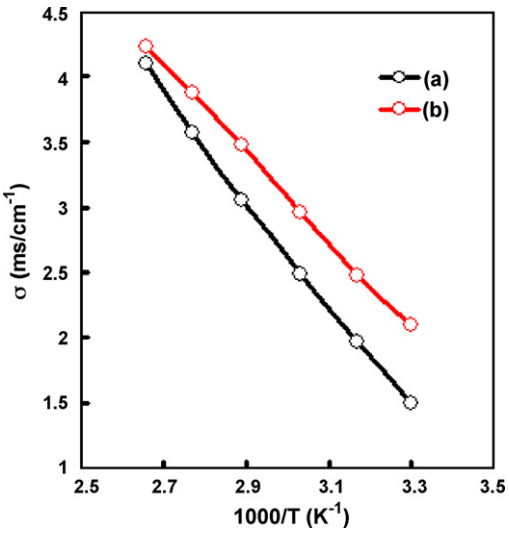

Fig. 12. Temperature dependence of ionic conductivity of polymer electrolyte (a) with and (b) without TiO_2 nano-particles.

4. Conclusions

Two soluble perylene-anthracene (A) and perylene-pyrene (P) compounds were synthesized from the condensation of the substituted perylene dianhydride with aminoanthracene and aminopyrene, respectively. Their T_g's were 124 °C for A and 75 °C for P. These compounds showed similar absorption spectra with optical band gaps of 2.05 eV. Their solutions emitted green-yellow light, while their films were not photoluminescent. We found that the compound A shows better photovoltaic response when used as the photo-sensitizer in a DSSC. The increase in power conversion efficiency of the DSSC with Al_2O_3 modified TiO_2 photoelectrode is attributed to the increased amount of dye adsorbed by the surface and longer electron lifetime. The modified Al_2O_3 shifts the conduction band potential towards negative direction also resulting in enhancement of the power conversion efficiency. The incorporation of TiO_2 nano-fillers in the polymer gel electrolyte further increases the power conversion efficiency of the DSSC, which is attributed to the enhanced ion transport in the polymer electrolyte. The higher ionic conductivity and lower activation energy of polymer electrolyte with TiO_2 are also responsible for the enhancement in PCE of the DSSC with polymer electrolyte with TiO_2 nano-particles.

Acknowledgement

Authors (GDS and P. Suresh) greatly acknowledge the financial support from Department of Science and Technology, Govt. of India, New Delhi.

References

[1] M.A. Green, K. Emery, Y. Hisikawa, W. Warta, Prog. Photovoltaics 15 (2007) 425.
[2] B. O'Regan, M. Grätzel, Nature 353 (1991) 737.
[3] Y. Kim, S. Cook, S.M. Tuladhar, S.A. Choulis, J. Nelson, J.R. Durrant, D.D.C. Bradley, M. Giles, I. McCulloch, C.-S. Ha, M. Ree, Nat. Mater. 5 (2006) 197.
[4] M. Gratzel, Prog. Photovoltaics 14 (2006) 429.
[5] H.J. Snaith, S.M. Zakeeruddin, Q. Wang, P. Pechy, M. Grätzel, Nano Lett. 6 (2006) 2000.
[6] K. Wessels, M. Maekawa, J. Rathousky, T. Oekermann, Thin Solid Films 515 (2007) 6497.
[7] D. Kuang, P. Wang, S. Ito, S.M. Zakeeruddin, M. Grätzel, J. Am. Chem. Soc. 128 (2006) 7732.

[8] M. Dürr, A. Schmid, M. Obermaier, S. Rosselli, A. Yasuda, G. Nelles, Nat. Mater. 4 (2005) 607.
[9] G.K. Mor, K. Shankar, M. Paulose, O.K. Varghese, C.A. Grimes, Nano Lett. 6 (2006) 215.
[10] E. Hosono, S. Fujihara, I. Honma, H. Zhou, Adv. Mater. 17 (2005) 2091.
[11] B.A. Gregg, J. Phys. Chem. B107 (2003) 4688.
[12] M. Grätzel, Inorg. Chem. 44 (2005) 6841.
[13] J.R. Durrant, S.A. Haque, E. Palomares, Chem. Commun. (2006) 3279.
[14] S. Kim, J.K. Lee, S.O. Kang, J. Ko, J.H. Yum, S. Fantacci, F. De Angelis, D. Di Censo, M.K. Nazeeruddin, M. Grätzel, J. Am. Chem. Soc. 128 (2006) 16701.
[15] N. Koumura, Z.S. Wang, S. Mori, M. Miyashita, E. Suzuki, K. Hara, J. Am. Chem. Soc. 128 (2006) 14256.
[16] D.P. Hagberg, T. Edvinsson, T. Marinado, G. Boschloo, A. Hagfeldt, L. Sun, Chem. Commun. (2006) 2245.
[17] K. Hara, T. Sato, R. Katoh, A. Furube, T. Yoshihara, M. Murai, M. Kurashige, S. Ito, A. Shinpo, S. Suga, H. Arakawa, Adv. Funct. Mater. 15 (2005) 246.
[18] M. Liang, W. Xu, F. Cai, P. Chen, B. Peng, J. Chen, Z. Li, J. Phys. Chem. C 111 (2007) 4465.
[19] N. Koumura, Z.-S. Wang, S. Mori, M. Miyashita, E. Suzuki, K. Hara, J. Am. Chem. Soc. 128 (2006) 14256.
[20] I. Jung, J.K. Lee, K.H. Song, K. Song, S.O. Kang, J. Ko, J. Org. Chem. 72 (2007) 3652.
[21] S. Kim, H. Choi, D. Kim, K. Song, S.O. Kang, J. Ko, Tetrahedron 63 (2007) 9206.
[22] C. Ego, D. Marsitzky, S. Becker, J. Zhang, A.C. Grimsdale, H. Mullen, J.D. MacKenzie, C. Silva, R.H. Friend, J. Am. Chem. Soc. 125 (2003) 437.
[23] W.S. Shin, H.H. Jeong, M.K. Kim, S.H. Jin, M.R. Kim, J.K. Lee, J.W. Lee, Y.S. Gal, J. Mater. Chem. 16 (2006) 384.
[24] L. Zang, R. Liu, M.W. Holman, K.T. Nguyen, D.M. Adams, J. Am. Chem. Soc. 124 (2002) 10640.
[25] H. Tian, P.H. Liu, W. Zhu, E. Gao, D.J. Wu, S. Cai, J. Mater. Chem. 10 (2000) 2708.
[26] H. Tian, P.H. Liu, F.S. Meng, E. Gao, S. Cai, Synth. Met. 121 (2001) 1557.
[27] S. Ferrere, B.A. Gregg, New J. Chem. 26 (2006) 1155.
[28] J. Cao, J.Z. Sun, J. Hong, X.G. Yang, H.Z. Chen, M. Wang, Appl. Phys. Lett. 83 (2003) 1896.
[29] Y. Shibano, T. Umeyama, Y. Matano, H. Imahori, Org. Lett 9 (2007) 1971.
[30] C. Zafer, M. Kus, G. Turkmen, H. Dincalp, S. Demic, B. Kuban, Y. Teoman, S. Icli, Sol. Energy Mater. Sol. Cells 91 (2007) 427.
[31] T.D.M. Bell, A. Stefan, S. Masuo, T. Vosch, M. Lor, M. Cotlet, J. Hofkens, S. Bernhardt, K. Müllen, M. van der Auweraer, J.W. Verhoeven, F.C. De Schryver, Chem. Phys. Chem. 6 (2005) 942.
[32] E.H.A. Beckers, S.C.J. Meskers, A.P.H.J. Schenning, Z. Chen, F. Würthner, R.A.J. Janssen, J. Phys. Chem. A 108 (2004) 6933.
[33] L. Valentini, D. Bagnis, A. Marrocchi, M. Seri, A. Taticchi, J.M. Kenny, Chem. Mater. 20 (2008) 32.
[34] W.Z. Yuan, J.Z. Sun, Y. Dong, M. Haeussler, F. Yang, H.P. Xu, A. Qin, J.W.Y. Lam, Q. Zheng, B.Z. Tang, Macromolecules 39 (2006) 8011.
[35] F. Würthner, V. Stepanenko, Z. Chen, C.R. Saha-Möller, N. Kocher, D. Dietmar Stalke, J. Org. Chem. 69 (2004) 7933.
[36] S. Koyuncu, M. Kus, S. Demic, I. Kaya, E. Ozdemir, S. Icli, J. Polym. Sci. Part A: Polym. Chem. 46 (2008) 1974.
[37] H. Adams, R.A. Bawa, K.G. McMillan, S. Jones, Tetrahedron: Asymmetry 18 (2007) 1003.
[38] (a) S.-T. Lin, Y.-F. Jih, P.P. Fu, J. Org. Chem. 61 (1996) 5271;
(b) H. Jung, A.U. Shaikh, R.H. Helfich, P.P. Fu, Environ. Mol. Mutagen. 17 (1991) 169.
[39] B.K. Banik, M. Suhendra, I. Banik, F.F. Becker, Synth. Commun. 30 (2000) 3745.
[40] B. Li, L.D. Wang, D.Q. Zhang, Y. Qiu, Chin. Sci. Bull. 49 (2004) 123.
[41] S. Chen, Y. Liu, W. Qiu, X. Sun, Y. Ma, D. Zhu, Chem. Mater. 17 (2005) 2208.
[42] H.S. Jung, J.K. Lee, M. Nastasi, S.W. Lee, J.Y. Kim, J.S. Park, K.S. Hong, H. Shin, Langmuir 21 (2005) 10332.
[43] Z. Liu, K. Pan, M. Liu, M. Wang, Q. Lü, J. Li, Y. Bai, T. Li, Electrochim. Acta 50 (2005) 2583.
[44] X. Zhang, I. Sutanto, T. Taguchi, K. Tokuhiro, Q. Meng, T.N. Rao, A. Fujishima, H. Watanabe, T. Nakamori, M. Uragami, Sol. Energy Mater. Sol. Cells 80 (2003) 315.
[45] Y. Diamant, S. Chappel, S.G. Chen, O. Melamed, A. Zaban, Coord. Chem. Rev. 248 (2004) 1271.
[46] Y. Diamant, S.G. Chen, O. Melamed, A. Zaban, J. Phys. Chem. B 107 (2003) 1977.
[47] J. Bisquert, J. Phys. Chem. B 106 (2002) 325.
[48] Q. Wang, J.E. Moser, M. Gratzel, J. Phys. Chem. B 109 (2002) 14945.
[49] D. Zhao, T. Feng, L. Lu, P. Cai, P. Jiang, Z. Blan, J. Phys. Chem. C 112 (2008) 8486.
[50] R. Kern, R. Sastrawan, J. Ferber, R. Stangel, J. Luther, Electrochim. Acta 47 (2002) 4213.
[51] H. Usual, H. Matsui, N. Tanabe, S. Yanagida, J. Photochem. Photobiol. A: Chem. 164 (2004) 97.
[52] M.S. Kang, K.S. Ahn, J.W. Lee, J. Power Sources 180 (2008) 896.
[53] A. Hegfeldt, M. Gratzel, Chem. Rev. 95 (1995) 49.
[54] J. Shi, S. Peng, J. Pei, Y. Liang, F. Cheng, J. Chen, ACS Appl. Mater. Interfaces 1 (2009) 944.
[55] J. Bisquert, Phys. Chem. Chem. Phys 10 (2008) 3175.
[56] C. He, L. Zhao, Z. Zheng, F. Lu, J. Phys. Chem. C 112 (2008) 18730.